Effective shear displacement on lateral adhesion force of a liquid bridge between separated plates

Tribology Letters

Effective Shear Displacement on Lateral Adhesion Force of a Liquid Bridge between Separated Plates

--Manuscript Draft--

Manuscript Number:	TRIL-D-16-00130R2
Full Title:	Effective Shear Displacement on Lateral Adhesion Force of a Liquid Bridge between Separated Plates
Article Type:	Article
Keywords:	liquid bridge; contact line; surface tension; adhesion; effective shear displacement; pinning
Corresponding Author:	Kentaro Tanaka, D. of Eng. Tokyo University of Marine Science and Technology Koto-ku, Tokyo JAPAN
Corresponding Author Secondary Information:	
Corresponding Author's Institution:	Tokyo University of Marine Science and Technology
Corresponding Author's Secondary Institution:	
First Author:	Kentaro Tanaka, D. of Eng.
First Author Secondary Information:	
Order of Authors:	Kentaro Tanaka, D. of Eng. Katsumi Iwamoto, D. of Eng.
Order of Authors Secondary Information:	
Funding Information:	JSPS KAKENHI (15562555) — Prof. Kentaro Tanaka JSPS KAKENHI (13274453) — Prof. Kentaro Tanaka
Abstract:	Adhesion force is among the most influencing factors in micro and nano-mechanics. A liquid bridge between two bodies gives rise to the adhesion force, which usually acts as additional normal load. However, the adhesion force acts also in lateral. We measured the lateral adhesion force of a sheared liquid bridge between parallel plates. In addition, movement of contact lines is tracked by using an image-processing technique, which allowed us to introduce an effective shear displacement. The lateral adhesion force has a linear relation with the effective shear displacement. It shows good agreement between experimental result and the analytical approach regarding changes of interfacial energy with simple rectangular shape of the liquid bridge. We further revealed that there is no contact line in pinned state even in the case with the very beginning of the sheared process. In this regard, however the contact line on rougher surface is awkward in its movement. Therefore, the liquid bridge between two rougher surfaces has higher effective shear displacement, and it results in the higher lateral adhesion force.
Response to Reviewers:	

Abstract

Adhesion force is among the most influencing factors in micro and nano-mechanics. A liquid bridge between two bodies gives rise to the adhesion force, which usually acts as additional normal load. However, the adhesion force acts also in lateral. We measured the lateral adhesion force of a sheared liquid bridge between parallel plates. In addition, movement of contact lines is tracked by using an image-processing technique, which allowed us to introduce an effective shear displacement. The lateral adhesion force has a linear relation with the effective shear displacement. It shows good agreement between experimental result and the analytical approach regarding changes of interfacial energy with simple rectangular shape of the liquid bridge. We further revealed that there is no contact line in pinned state even in the case with the very beginning of the sheared process. In this regard, however the contact line on rougher surface is awkward in its movement. Therefore, the liquid bridge between two rougher surfaces has higher effective shear displacement, and it results in the higher lateral adhesion force.

Keywords liquid bridge; contact line; surface tension; adhesion; effective shear displacement; pinning (6 keywords)

1. Introduction

It is easier to open a plastic bag with wet fingers. Adhesive force originates from capillary force due to liquid enhances skin friction [1] and allows you to open closely attached plastic sheets in two. In a presence of liquid film, droplets or condensed water from humid air on a surface, a liquid bridge can be formed between two bodies. The liquid bridge gives rise to the adhesion force between the bodies, which acts as additional normal load and results in an increase in friction force. While the adhesion force is relatively weak in macroscopic scales, it is among the most influencing factors in micro and nano-mechanics [2,3]. With recent advances in ultrafine processing technologies, mechanical devices can be designed as smaller. However, because of the high friction force and subsequent excessive wear, these micro mechanical devices, e.g. micro-rotors result in lifetimes too short for many applications [4].

Owing to surface tension and contact angle hysteresis, the adhesion force acts also in lateral [5]. While typical friction force is generated in solid-solid contacts, the adhesive lateral force can act without it. Here, the adhesive lateral force required to relative lateral movement of two separated surfaces with liquid bridge intervening, is called as the lateral adhesion force. The situations can be found in flip chip bonding [6, 7], die coating [8], droplet bearing [9] and also in studies of friction in skiing [10, 11]. When the liquid bridge is sheared by the relative lateral movement of surfaces, first the liquid bridge will deform with change in liquid-air interface. Then, the contact area of the liquid bridge will start to slide relative to a surface [5] with change in solid-liquid (and solid-air) interface. This description can explain a linear response of the lateral adhesion force during early stage of liquid bridge shearing [7], and subsequent steady state [5]. To the best of our knowledge, analytical models based on the above description are not sufficient to coincide quantitatively with experiments. Only a few reports show qualitative agreement between them, in case within a very small shear displacement with a constraint of contact line movement by edges [12].

In this study, the lateral adhesion force during sheared process of the liquid bridge between parallel plates was measured. Movement of contact line, meeting point of air, liquid and solid phases, was also observed by using an image processing technique. Acquired data allows us to reveal a relation between the lateral adhesion force and an effective shear displacement. The relation can be qualitatively compared with theoretical estimation by a simple analytical model. Effect of surface roughness was also discussed. It has an important role on sliding behavior of liquid-solid interface.

2. Analytical model

Behavior of the liquid bridge under shearing is dependent on a state of the contact line. Depinned state allows contact line to move. On the other hand, pinned contact line does not move. In most cases, the contact lines are considered to be pinned to the surface during early stage of a lateral action [6,13]. Fig. 1(a) illustrates the liquid bridge deformation by the relative lateral movement of surfaces with the pinned contact lines. In this case, change in liquid-air interfacial area is needed to estimate the force required to the lateral movement, we assume rectangular column as the liquid-air interface's shape (Fig. 2). This simplified model has a discrepancy with the meniscus interface of an actual liquid bridge. However, the difference in resultant lateral adhesion force is very small, especially in small shear displacement [7]. The liquid-air interfacial area under shear deformation is

$$S_{\mathrm{LA}} = 2lh + 2w\sqrt{u^2 + h^2}$$

with *l*, *h*, *w* and *u* denoting the length, height, width of the liquid bridge and its shear displacement. The force acts by the change in the liquid-air interfacial free energy $E_{\mathrm{LA}}(= \gamma_{\mathrm{LA}} S_{\mathrm{LA}})$ can be calculated as

$$F_{\mathrm{pin}} = -\frac{\mathrm{d}E_{\mathrm{LA}}}{\mathrm{d}u} = -\gamma_{\mathrm{LA}} \frac{\mathrm{d}S_{\mathrm{LA}}}{\mathrm{d}u} = -2\gamma_{\mathrm{LA}} \frac{wu}{\sqrt{u^2 + h^2}}$$

with the surface tension γ_{LA}[7]. Assuming small shear displacement ($u/h \ll 1$), the force simplifies to $F_{\mathrm{pin}} = -2\gamma_{\mathrm{LA}}\, wu/h$. The force required to the lateral movement ($-F_{\mathrm{pin}}$) with pinned contact lines linearly increases with shear displacement. With this model, the force is dependent on the size, *w*, *h* of the liquid bridge. For example, in case with larger *h* , because of the liquid bridge keeps constant volume, *l* and *w* should become smaller. Therefore, the force become smaller. The dependence of the height of the liquid bridge have pre-experimentally confirmed as the model described here.

When a contact line depins from the surface and slides relative to a surface with a contact angle θ as illustrated in Fig. 3, change in interfacial energy per unit length should be counted as

$$dE/w = \gamma_{\mathrm{SL}} dx - \gamma_{\mathrm{SA}} dx + \gamma_{\mathrm{LA}}\, dx \cos\theta$$
$$= \gamma_{\mathrm{LA}} (\cos\theta - \cos\theta_{\mathrm{E}})\, dx$$

where dx is displacement of the contact line, and θ_{E} is the equilibrium contact angle given by the Young's equation ($\gamma_{\mathrm{SL}} - \gamma_{\mathrm{SA}} + \gamma_{\mathrm{LA}} \cos\theta_{\mathrm{E}} = 0$) [14]. Suppose that the liquid bridge starts to slide relative to a bottom surface as in Fig. 1(b). With different contact angles θ_{r} and θ_{l} at right and left

side of contact lines, the force per unit length is calculated as

$$F_{\mathrm{depin}}/w = -\frac{\mathrm{d}(E_{\mathrm{r}}/w + E_{\mathrm{l}}/w)}{\mathrm{d}x} = -\{\gamma_{\mathrm{LA}}(\cos\theta_{\mathrm{r}} - \cos\theta_{\mathrm{E}}) - \gamma_{\mathrm{LA}}(\cos\theta_{\mathrm{l}} - \cos\theta_{\mathrm{E}})\}$$

$$= -\gamma_{\mathrm{LA}}(\cos\theta_{\mathrm{r}} - \cos\theta_{\mathrm{l}})$$

The force required to the relative sliding with depinned contact lines is proportional to the difference of contact angles ($\cos\theta_{\mathrm{r}} - \cos\theta_{\mathrm{l}}$). This formula accords with the well-known force from contact angle hysteresis (difference in contact angle between advancing and receding contact line) [15]. As long as the liquid bridge keeps its shape, the force keeps constant. Furthermore, in case with the rectangular column bridge model, following relations can be used

$$\cos\theta_{\mathrm{l}} = \cos(\pi - \theta_{\mathrm{r}}) = -\cos\theta_{\mathrm{r}}$$

$$\cos\theta_{\mathrm{r}} = \frac{u}{\sqrt{u^2 + h^2}}$$

Then, the relation

$$F_{\mathrm{depin}} = -2\gamma_{\mathrm{LA}}\frac{wu}{\sqrt{u^2 + h^2}} = F_{\mathrm{pin}}$$

is obtained. This means that the force during a pinned-depinned transition remains unchanged.

On the other hand, in case with release of retention of liquid-air interfacial energy with depinned contact line as illustrated in Fig. 1(c), the force will drop. However, such situation did not appear in our experiment.

3. Experimental section

3.1. Apparatus

The experimental system is shown schematically in Fig. 4. The liquid bridge forms between flat plates. The bottom plate is on an automatically operated micrometer stage. The top plate is supported with a parallel leaf spring, which can be moved vertically by a manually operated micro stage. While the bottom plate moves laterally by the micrometer stage, the lateral force acts on the top plate is measured from a deflection of the parallel leaf spring via a non-contact capacitive displacement sensor. The spring constant is 408N/m. The sensor resolution is 1nm. The force resolution of our apparatus with the above presented components is below 0.5 μN. The measurement system is placed between a diffusive sheet with a white light and a CCD camera with a microscope. Thus, a shadowgraph of the

liquid bridge can be captured. The frame rate of the camera is 100 frame/s.

3.2. Position tracking of contact line

Change in position of contact lines of the liquid bridge are tracked by using an image-processing technique. Feature tracking method with Lucas-Kanade algorithm [16] is coded with OpenCV libraries. This method can estimate a position translation from given two subsequent frames. Positions of four contact lines and two plates are tracked. From a comparison with the bottom plate displacement measured by the displacement sensor, error of the tracked position with this method is about 2%.

3.3. Materials and test condition

In this study, distilled water was used as the liquid bridge. Glass plates, which have optically flat surface and frosted surface were prepared. The flat and frosted surfaces have surface roughness in *Ra* of 3nm and 60nm respectively. The plates are made of BK7 glass. Before experiment, the both plates are cleaned by ultrasonic cleaning with an ethanol bath.

A water liquid bridge of 10μL volume formed between plates with 1.0mm±0.05mm separation. From the stationary situation, the bottom plate starts to move with a constant speed, 20μm/s. Experiment is repeated 5 times for each condition. All experiments were performed in standard laboratory conditions, temperature of about 25 ˚C and relative humidity of about 60%.

4. Results and discussion

4.1. Effective shear displacement

The result of a single measurement of the liquid bridge between two smoothed (*Ra* 3nm) plates is shown in Fig. 5 and Fig. 6. The lateral adhesion force with the bottom plate displacement is plotted in Fig. 6(a). The force linearly increases during early stage of the shearing process, and then reaches a steady state. Here, we define the linear limit of the force (blue filled circle in Fig. 6(a)) at a point where the force becomes 10% smaller than a linear fitted line (gray line in Fig. 6(a)). Maximum of the force, $F_{\max}$ is calculated by time-average in the steady state. The lateral adhesion force and the bottom plate displacement shows a good linearity in the linear range, its slope is about 0.15 N/m. This value does not match the slope of the analytical model for square shape in cross section of the liquid bridge, $2\gamma_{\mathrm{LA}}\, w/h = 0.46\ \mathrm{N/m}$ ($\because\ lwh = 10\mu\mathrm{L},\ l = w = 3.2\mathrm{mm}$). The slope depends on the width, w of the liquid bridge, which cannot be measured with our measurement. Actually, contact area elongated in shearing direction, average length is about 4.6mm (w= 2.2mm). In this case, the slope becomes

about 0.32N/m. In either case, the slope of the measurement is smaller than the half that of the analytical model. There is a difference between the bottom plate displacement in the experiment and the shear displacement, u in the analytical model.

Movement of contact lines are well tracked with the feature tracking method. By comparing these tracked positions with its initial positions, which are shown in white allows in Fig. 5, displacement of contact lines can be calculated as shown in Fig. 6(b). In the linear range of the lateral adhesion force, contact lines at bottom right (BR) and bottom left (BL) position seem to follow the movement of the bottom plate. These positions are linearly increases with the displacement of the bottom plate. However, sliding of contact area relative to the bottom plate, which can be calculated from the relative displacement of the center of the contact area to the plate, occurs from the very beginning of the sheared process (see Fig. 6(c)). The centers are indicated by lines with a gray open square and a black filled circle in the bottom snapshots of Fig. 5. Situations that allows contact lines fully pinned to the plate surface during early stage of a lateral action [13] are not observed. Hence, the bottom plate displacement does not equal to the shear displacement. Therefore, we introduce an effective shear displacement, which is defined by the difference between the centers of each contact areas. The effective shear displacement, u_{eff} in Fig. 6(d) has a similar profile with the lateral adhesion force. We can find a linear relation between the lateral adhesion force and the effective shear displacement (Fig. 7). The slope of the linear fitted line is 0.39 N/m. This value agrees well with the analytical estimation above.

4.2. Effect of surface roughness on relative sliding of contact area

Experiments of rougher surface roughness are carried out with the plate of frosted surface. Its roughness in *Ra* is 20 times higher than the one of the smooth surface. We prepared two roughness combinations of plates, in addition to the smooth-smooth combination. One is which the bottom plate is replaced with the plate of the rougher surface. Another is which the both top and bottom plates are replaced with them. Fig. 8 shows all the result of sliding of contact area relative to the plates. First, in all cases, which include the case with the rough surface of the bottom plate, the sliding occurs from the very beginning of the sheared process and occurs at interface with the bottom plate. This implies that under our experimental condition, there is no contact line in pinned state, and the inertial action by the bottom plate motion initiates the sliding. In case with the smooth-smooth combination, there

are two trends. It shows similar trend with Fig. 6(c) that three times out of five experiments as shown with red, gray and black line in Fig. 8(a) and in all times of the rough-rough combination in Fig. 8(c). The sliding relative to the bottom plate is always dominant until the equilibrium stage from the early stage of the sheared process. On the other hand, in two times of the smooth-smooth combination as shown with blue and green line in Fig. 8(a) and in all times of the smooth-rough combination in Fig. 8(b), we found that dominant sliding transfer from the bottom to the top. The rougher bottom surface hinders keeping the sliding on the bottom. Sometimes, a defect or a contamination on the smooth bottom surface of the smooth-smooth combination may have same effect of the rougher bottom surface. However, in case with the rough-rough combination, there is no advantage in the dominant sliding transfer from the rough surface to the rough. The effect of contamination is behind the roughness of the rougher surface. In this regard, however the contact line on the rougher surface is actually awkward in its movement. The rough-rough combination leads to higher effective shear displacement and results in higher lateral adhesion force than the smooth-rough combination, which shows almost same value as the smooth-smooth combination (Fig. 9).

5. Conclusions

With our apparatus, the lateral adhesion force of liquid bridge between parallel plates can be measured. In addition, position tracking of contact lines allows us to calculate the effective shear displacement. It shows good agreement between the analytical estimation based on changes in interfacial energy with a simple rectangular column bridge model and the experimental result with the effective shear displacement. The lateral adhesion force has linear relation with the effective shear displacement. Moreover, we observe the fact that there is no contact line in fully pinned state. With the depinned state, sliding of contact area relative to the plate occurs from the very beginning of the sheared process. Maximum of the lateral adhesion force depends on the combination of the roughness of two plates. The rough-rough combination leads to higher effective shear displacement and results in higher lateral adhesion force than the smooth-smooth and the smooth-rough combination. In the latter cases, system choose interface with smoother surface roughness for sliding of contact area.

Acknowledgments

This work was supported by JSPS KAKENHI Grant Numbers 15562555 and 13274453.

References

[1] Derler, S. , Gerhardt , L.-C.: Tribology of Skin: Review and Analysis of Experimental Results for the Friction Coefficient of Human Skin. Tribol. Lett. 45, 1-27 (2012)

[2] Mate, C. M.: Tribology on the Small Scale: A Bottom Up Approach to Friction, Lubrication, and Wear (Mesoscopic Physics and Nanotechnology). Oxford University Press, New York (2008)

[3] Perrson, B. N. J.: Sliding Friction: Physical Principles and Applications 2nd ed.. Springer, New York (2000)

[4] Zhang, W., Meng, G., Li, H.: Electrostatic Micromotor and Its Reliability. Microelectron. Reliab. 45, 1230-1242 (2005)

[5] Pilat, D. W., Papadopoulos, P., Schäffel, D., Vollmer, D., Berger, R., Butt, H.-J.: Dynamic Measurement of the Force Required to Move a Liquid Drop on a Solid Surface. Langmuir 28, 16812-16820 (2012)

[6] Yost, B., McGroarty, J., Børgesen, P., Li, C. Y.: Shape of a Nonaxisymmetric Liquid Solder Drop Constrained by Parallel Plates. IEEE T. Compon. Hybr. 16, 523-526 (1993)

[7] Lambert, P., Mastrangeli, M., Valsamis, J.-B., Degrez, G.: Spectral Analysis and Experimental Study of Lateral Capillary Dynamics for Flip-chip Applications. Microfluid. Nanofluid. 9, 797–807 (2010)

[8] Chang, Y.-R., Chang, H.-M., Lina, C.-F., Liua, T.-J., Wuatsuoka, P.-Y.: Three Minimum Wet Thickness Regions of Slot Die Coating. J. of Colloid Interf. Sci. 308, 222–230 (2007)

[9] Suzuki, K., Uyeda, Y.: Load-carrying Capacity and Friction Characteristics of a Water Droplet on Hydrophobic Surfaces. Tribol. Lett. 15, 77-82 (2003)

[10] Bowden, F. P.: Friction on Snow Ice. Proc. R. Soc. Lond. Ser-A 217, 462-478 (1953)

[11] Colbeck, S. C.: The Kinetic Friction of Snow. J. of Glaciol. 34 ,78-86 (1988)

[12] Mastrangeli, M., Valsamis, J.-B., Van Hoof, C., Celis, J.-P., Lambert, P.: Lateral Capillary Forces of Cylindrical Fluid Menisci: A Comprehensive Quasi-static Study. J. Micromech. Microeng. 20, 075041 (2010)

[13] Mastrangeli, M., Arutinov, G., Smits, E. C. P., Lambert, P.: Modeling Capillary Forces for Large Displacements. Microfluid. Nanofluid. 18, 695–708 (2015)

[14] de Gennes, P.-G., Brochard-Wyart, F., Quéré, D.: Capillarity and Wetting Phenomena, Drops,

Bubbles, Pearls, Waves. Springer, New York (2004)

[15] Furmidge, C. G. L.: Studies at Phase Interfaces, I. The Sliding of Liquid Drops on Solid Surfaces and a Theory for Spray Retention. J. of Colloid Sci. 17, 309-324 (1962)

[16] Lucas, B. D., Kanade, T.: An Iterative Image Registration Technique with an Application to Stereo Vision. Proc. of Int. Joint Conf. on Artificial Intelligence 674-679 (1981)

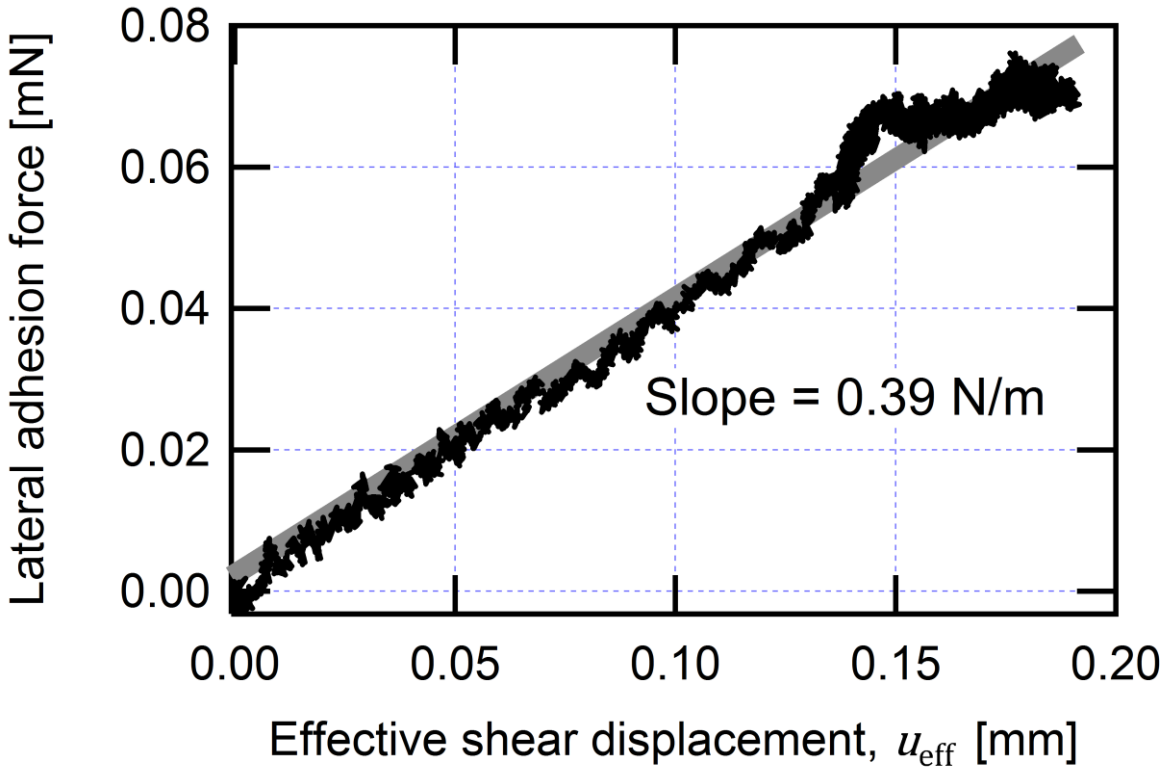
Lateral adhesion force [mN]
0.08
0.06
0.04
0.02
0.00
Slope = 0.39 N/m
0.00
0.05
0.10
0.15
0.20
Effective shear displacement, u_{eff} [mm]

Fig. 7

Title: Effective Shear Displacement on Lateral Adhesion Force of a Liquid Bridge between Separated Plates

Author: Kentaro Tanaka • Katsumi Iwamoto

Figure captions

Fig. 1 Schematic model of liquid bridge behavior with different state of contact line, **(a)** shear deformation with pinned contact lines, **(b)** sliding relative to a surface with depinned contact lines, **(c)** release of retention of shear deformation with depinned contact line. Filled circles represent pinned contact line and open circles represent depinned contact line.

Fig. 2 Analytical model of sheared liquid bridge with rectangular column

Fig. 3 Moving contact line with contact angle θ by a distance *dx*. Combinations of S, L, A denoted solid, liquid, air respectively, on the subscript of the interfacial tension γ symbols correspond to interfacial tensions between two phases.

Fig. 4 Schematic of experimental apparatus. Deformation of liquid bridge can be observed with CCD camera through a microscope, lateral adhesion force is measured by a deflection of a parallel leaf spring via a capacitive displacement sensor.

Fig. 5 Snapshots of the liquid bridge between glass plates under shear. Numeric with millimeter unit means the bottom plate displacement. Small green dots show tracked positions of contact line and specific point of plates by the feature tracking method. White arrows show initial positions of contact line. Open square and filled circle in the bottom snapshot represent the center position of contact area. Lateral difference of the centers corresponds to an effective shear displacement.

Fig. 6 Bottom plate displacement versus **(a)** lateral adhesion force, **(b)** displacement of contact lines, **(c)** sliding of contact area relative to the both plates and **(d)** effective shear displacement. A vertical dashed line indicates the linear range of the lateral adhesion force.

Fig. 7 Lateral adhesion force versus effective shear displacement. The gray line is the linear fitted line.

Fig. 8 Sliding of contact area relative to plates of **(a)** smooth-smooth combination **(b)** smooth(top) -rough (bottom) combination **(c)** rough-rough combination

Fig. 9 Maximum of lateral adhesion force versus maximum of effective shear displacement. Open marks represent the average of each roughness combinations.

Figures

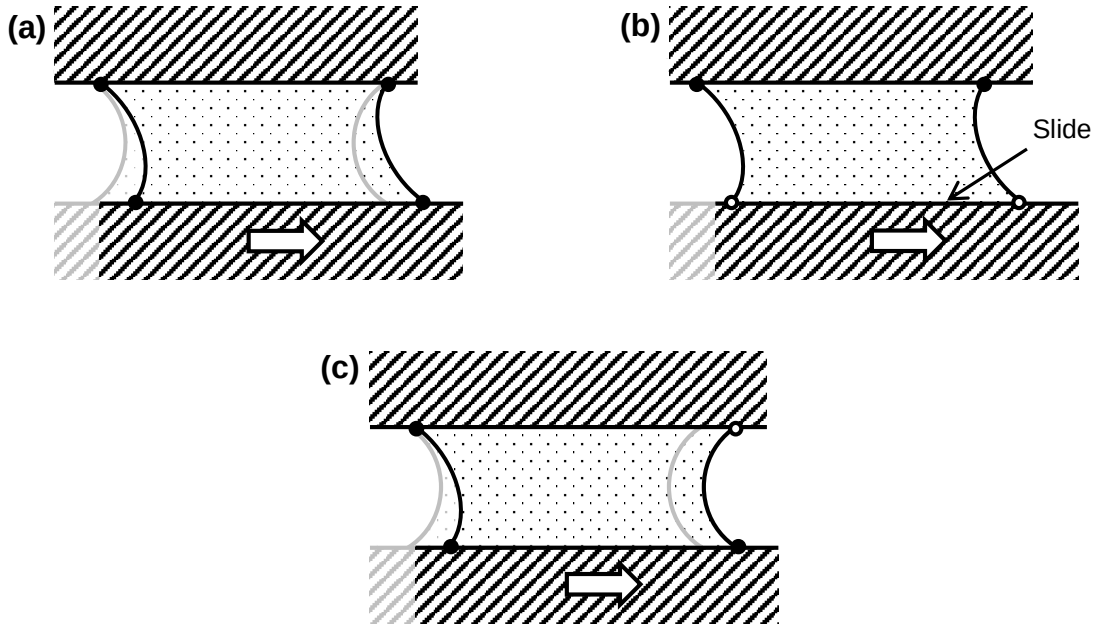

Fig. 1

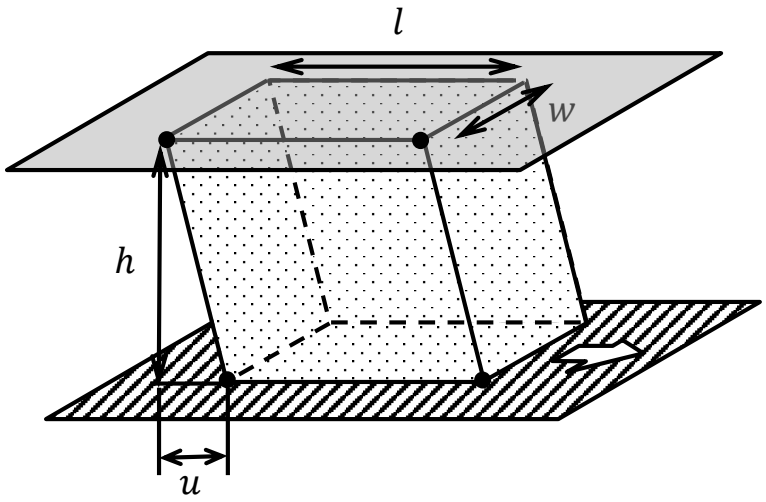

Fig. 2

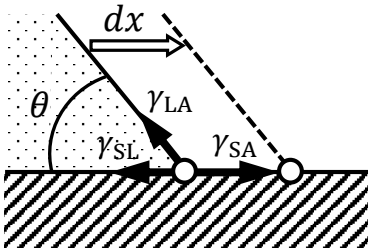

Fig. 3

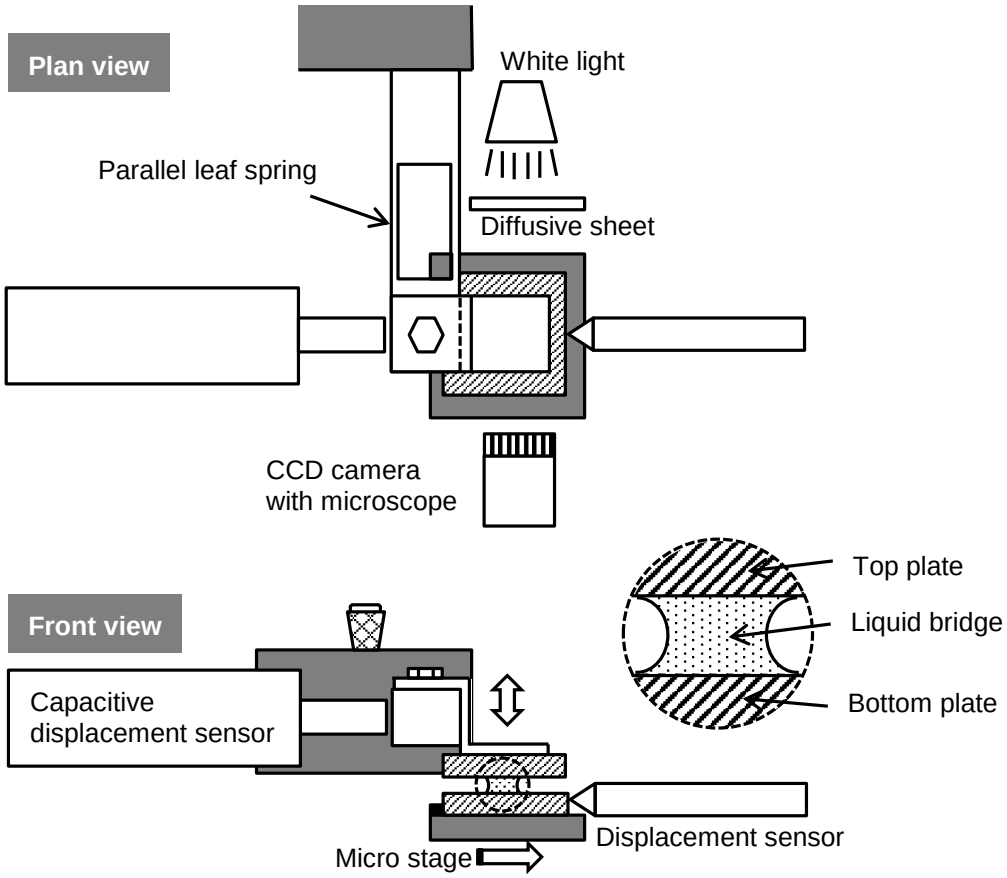
Plan view
White light
Parallel leaf spring
Diffusive sheet
CCD camera
with microscope
Top plate
Liquid bridge
Bottom plate
Front view
Capacitive
displacement sensor
Displacement sensor
Micro stage

Fig. 4

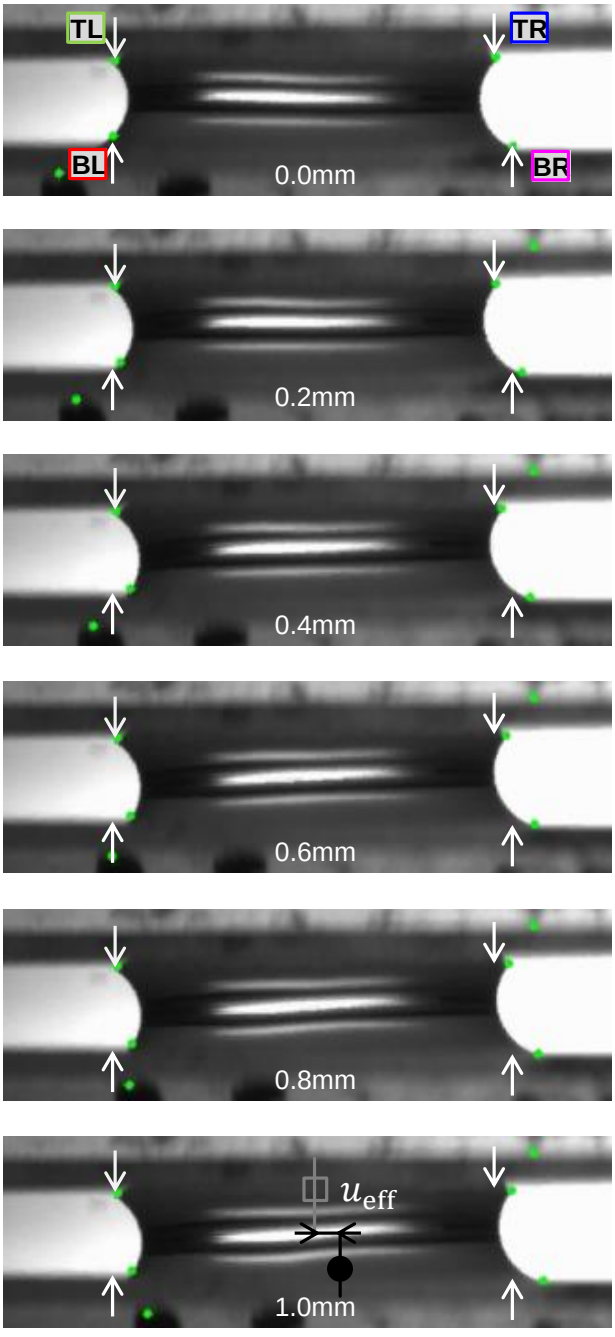

Fig. 5

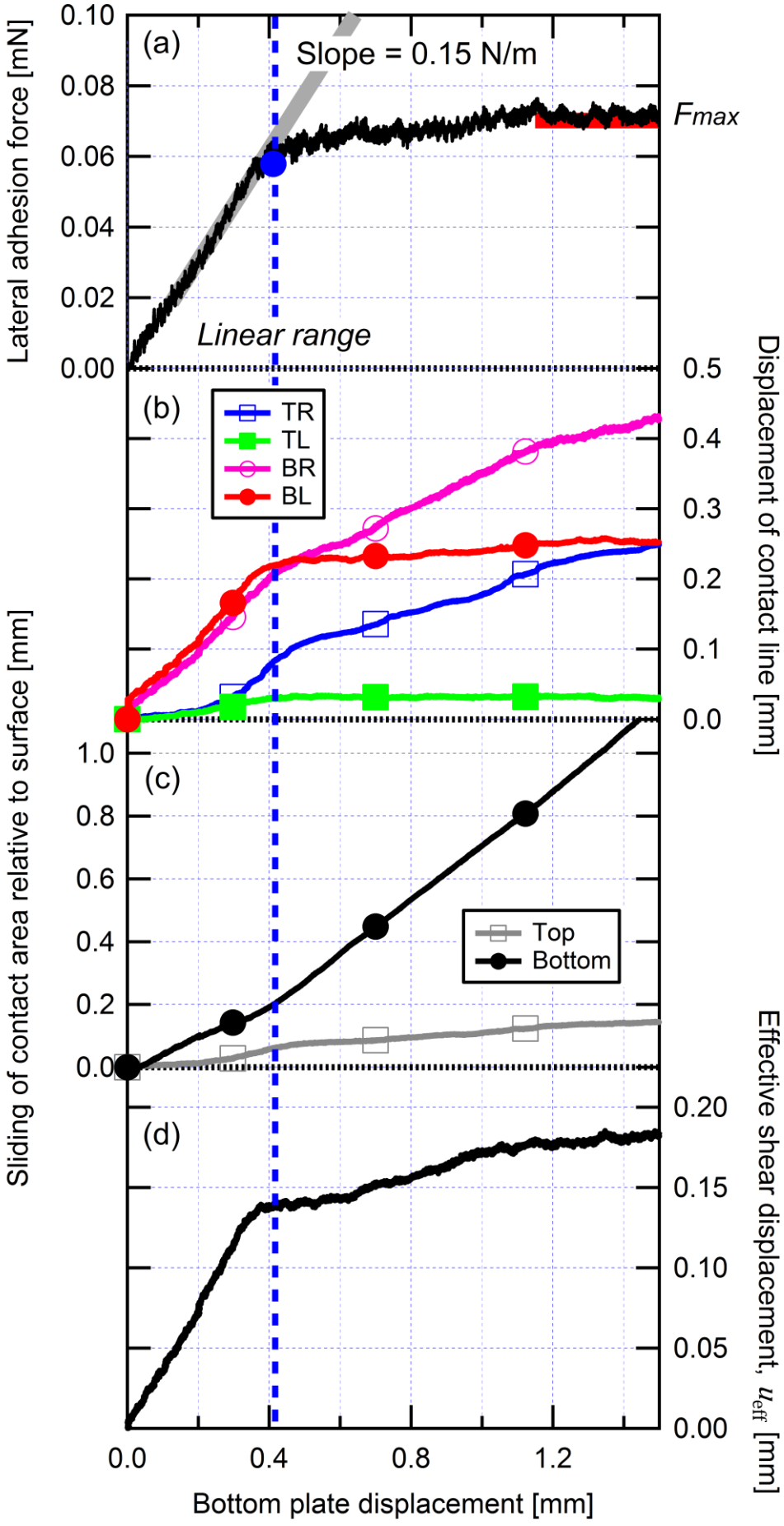
(a)
Slope = 0.15 N/m
Fmax
Linear range
Lateral adhesion force [mN]
0.10
0.08
0.06
0.04
0.02
0.00
(b)
TR
TL
BR
BL
Displacement of contact line [mm]
0.5
0.4
0.3
0.2
0.1
0.0
(c)
Top
Bottom
Sliding of contact area relative to surface [mm]
1.0
0.8
0.6
0.4
0.2
0.0
(d)
Effective shear displacement, u_{eff} [mm]
0.20
0.15
0.10
0.05
0.00
0.0
0.4
0.8
1.2
Bottom plate displacement [mm]

Fig. 6

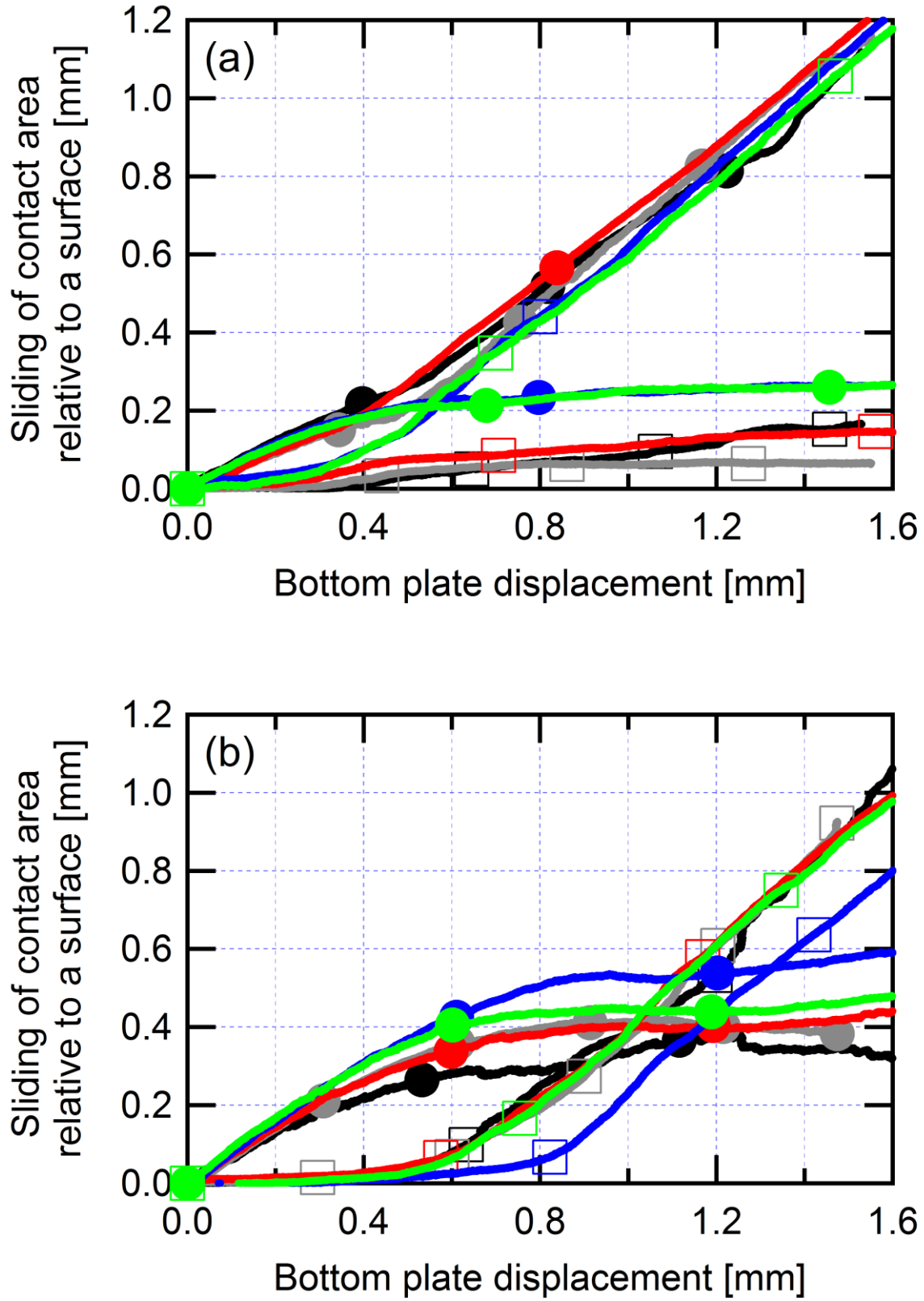
(a)
Sliding of contact area relative to a surface [mm]
Bottom plate displacement [mm]
0.0
0.2
0.4
0.6
0.8
1.0
1.2
0.0
0.4
0.8
1.2
1.6
(b)
Sliding of contact area relative to a surface [mm]
Bottom plate displacement [mm]

Fig. 8

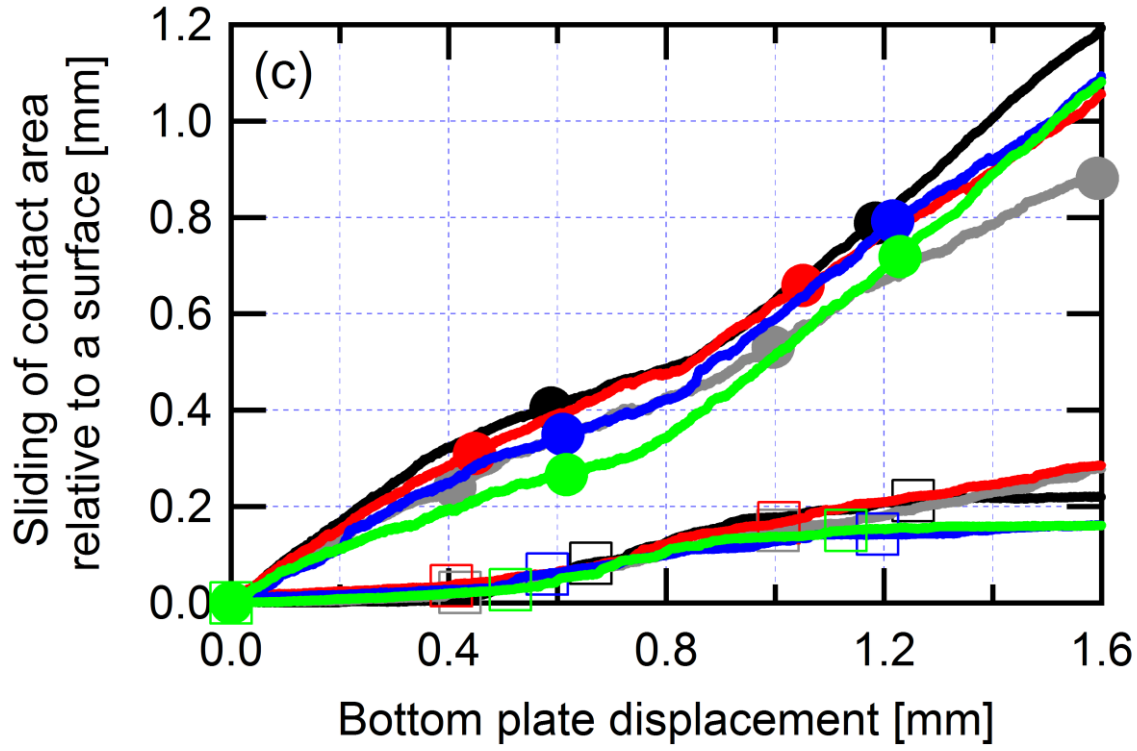
(c)
Sliding of contact area relative to a surface [mm]
Bottom plate displacement [mm]
0.0
0.2
0.4
0.6
0.8
1.0
1.2
0.0
0.4
0.8
1.2
1.6

Fig. 8

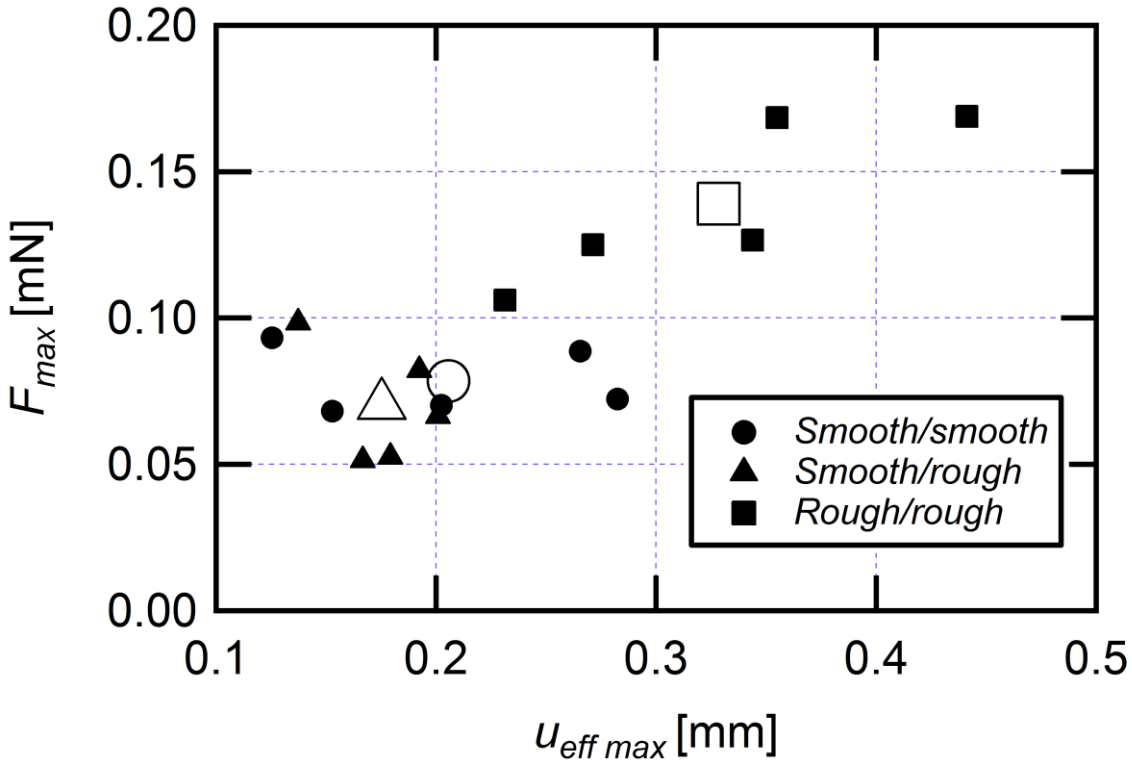
0.20
0.15
0.10
0.05
0.00
0.1
0.2
0.3
0.4
0.5
F_{max} [mN]
$u_{eff\ max}$ [mm]
Smooth/smooth
Smooth/rough
Rough/rough

Fig. 9